Simplistic Model for the Dendritic Growth of a Monolayer in Dip Pen Nanolithography

Hyojeong Kim,[†] George C. Schatz,[‡] and Joonkyung Jang*[,†]

Department of Nanomaterials Engineering, Pusan National University, Miryang, 627-706, Republic of Korea, and Department of Chemistry, Northwestern University, Evanston, Illinois 60208-3113

Received: October 12, 2009; Revised Manuscript Received: December 11, 2009

This paper presents a simple random-walk (RW) model for monolayer growth in dip pen nanolithography (DPN). The monolayer in the RW model grows via a combination of hopping down and serial pushing of molecules deposited from the tip. The directional coherence in pushing induces branches of a monolayer that grow in preferential directions that are determined by the underlying lattice for the surface. The RW model accurately reproduces a molecular dynamics (MD) simulation for the DPN of nonpolar molecules on gold-like surfaces, indicating that the pushing mechanism accurately describes molecular motions. The molecular deposition in the MD simulation is found to be close to a random Poisson process. The high directional coherence produces self-replicating branches in the monolayer that are characteristic of dendritic growth. With a change in directional coherence, the RW model produces diverse structures such as circles, hexagons, and dendrites.

1. Introduction

The dendritic growth of structures[1] has interested researchers in many areas, with applications to processes such as the solidification of supercooled liquids,[2,3] electropolymerization,[4] and epitaxial film growth.[5] It was recently reported that a dendritic monolayer of organic molecules can be grown by using a nanometer tip as a point source of molecular deposition.[6,7] In this dip pen nanolithography (DPN),[8,9] a tip continuously creates nanodroplets that subsequently spread to form a monolayer over a surface (Figure 1a). A micrometer-sized dendrite was observed in the DPN of dodecylamine[6] or polyethylene glycol[7] on mica. This is in stark contrast to the isotropic and circular monolayer patterns obtained with conventional DPN (e.g., alkanethiol on gold). A dendrite forms during the growth of a crystal or epitaxial film via diffusion limited aggregation (DLA)[5] of atoms or molecules that diffuse toward the periphery of a growing structure from the outside of the periphery. However, the molecules in DPN diffuse from the center to the periphery of a growing monolayer structure. Therefore, the dendritic growth in DPN cannot be explained by DLA.[5] The underlying mechanisms are currently unknown.

This paper reports that a dendritic monolayer in DPN can be generated by a simple random-walk (RW) model that is based on the physical intuition that a monolayer grows by the hopping down of a molecule on the top of other molecules or by a series of pushing steps initiated by molecules deposited from the tip. If the molecules move collectively in the same direction during serial pushing, the monolayer develops branches in certain selected directions that are determined by surface anisotropy. As this coherence in direction increases further, the monolayer begins to form self-developing branches that are characteristic of dendritic growth. To illustrate this, the RW model is applied to a generic class of DPN processes by using nonpolar organic molecules on a gold-like surface. The model quantitatively reproduces a monolayer pattern with hexagonal branches that is obtained from a molecular dynamics (MD) simulation which shows that the underlying algorithm associated with serial

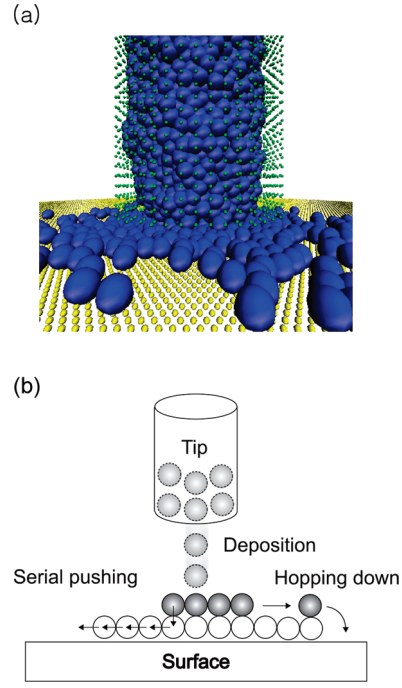

Figure 1. (a) MD simulation of DPN. Nonpolar spherical molecules are stacked inside a cylindrical tip and later form a monolayer on the (111) surface composed of gold-like atoms. The tip and surface atoms are drawn smaller for clarity. (b) Random walk model of DPN. Molecules deposited from the tip (drawn as dotted circles) create a droplet that spreads to become a monolayer later. The molecules (shaded circles) move on top of the other molecules (open circles) and hop down to the surface at the periphery (hopping down). Alternatively, a molecule (shaded circles) pushes down the molecule below it (open circles), and the molecule pushed out in turn pushes its neighbor out of place. This pushing propagates (drawn as left arrows) toward the periphery of the monolayer until there is no molecule left to push out (serial pushing).

* Corresponding author. E-mail: jkjang@pusan.ac.kr; Tel.: +82-55-350-5277; Fax.: +82-55-350-5653.
[†] Pusan National University.
[‡] Northwestern University.

10.1021/jp909766p
Published on Web 01/07/2010

pushing provides an accurate description of the physical system. In addition, the model produces a variety of structures such as circles, hexagons, and dendrites by simply changing the directional coherence in the serial pushing.

2. Details of Model and Simulation

Molecules in the RW model are assumed to execute RWs with a discrete time step on a three-dimensional lattice. A multilayered droplet such as that in Figure 1b is made of columns that are stacked continuously with molecules as in the solid-on-solid (SOS) model for crystal growth.[5] A molecule in the upper layer of the droplet is free to move and can hop down to the surface at the periphery, as shown in Figure 1b. This hopping-down mechanism, which is dominant for a molecule trapped irreversibly by the surface (such as in chemisorption), invariably gives isotropic circular monolayers.[10] The present RW model also includes the serial-pushing mechanism:[11] a molecule pushes down the molecule below it, which in turn pushes its neighbor out of place. This push-induced movement laterally propagates toward the periphery until there are no molecules left to push out. This sequence of push-induced movements is taken to occur without time delay on the time scale of the RW (because each push arises from a momentum transfer between colliding molecules and should occur much faster than diffusion). A molecule on the bare surface is allowed to move only if it is pushed by one of its nearest neighbors (NNs), above or beside it. Therefore, no voluntary hopping on the surface is allowed (if such a spontaneous surface diffusion is allowed, there will be no permanent monolayer at long times). A previous MD simulation[12] showed that this serial pushing process prevails provided that the lateral movement of a molecule from one binding site to its neighboring site on the surface is facile (even if the molecule-surface interaction is strong).

To implement the serial-pushing mechanism in a RW simulation, we need to decide in what direction a molecule should move if pushed by another molecule. If the pushing is directionally coherent, push-induced displacement propagates in the same direction as the initial pushing. This coherence develops branches of a monolayer in the preferential directions, for example, the six equivalent directions connecting the three-fold hollow sites of a (111) surface. However, if pushing is directionally incoherent, each consecutive displacement is independent and random, giving an isotropic circular monolayer. We define the directional coherence length N_d as the number of push-induced movements in the same direction (Figure 2). If the molecule initially pushes out its neighboring molecule, the subsequent $(N_d - 1)$ movements take the same direction as the initial pushing direction. The direction of the $(N_d + 1)^{th}$ molecular displacement becomes random, and then, the subsequent $(N_d - 1)$ movements are taken to occur in the same direction as the $(N_d + 1)^{th}$ displacement (Figure 2). This series of push-induced movements continues until it stops at the periphery (where there are no molecules left to push out). Note that N_d refers to the direction only, not the length, of a push-induced move (the length of each push-induced movement is always one lattice spacing as in RW moves). We further assume that N_d obeys the Poisson distribution,

$$P(N_d;\lambda) = \exp(-\lambda)\,\lambda^{N_d}/N_d! \quad (N_d = 1, 2, ...) \qquad (1)$$

where the parameter λ is the average of N_d and was chosen to match the MD simulation results (see below). N_d at each time step was determined by using a random number generator of $P(N_d;\lambda)$.

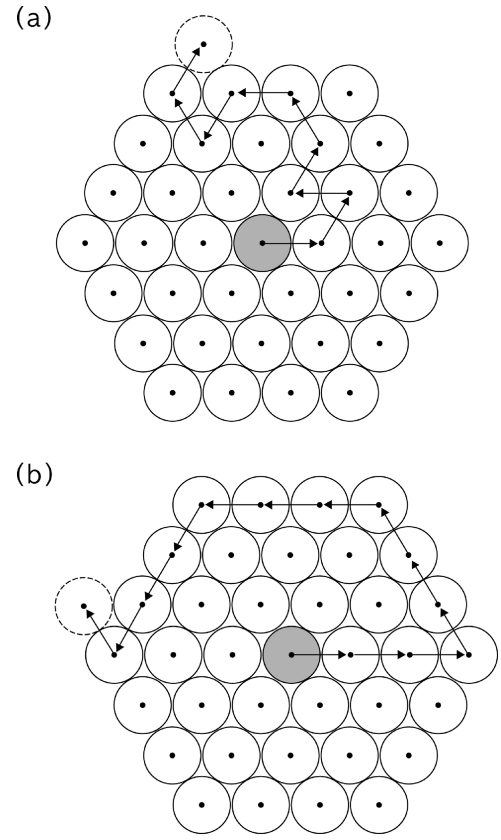

Figure 2. Serial-pushing events with different directional coherence lengths N_d. In each panel, the molecule drawn as a gray circle initiates a series of push-induced movements of molecules (open circles). The trigonal lattice sites are drawn as dots. The initial pushing propagates in the direction of arrows. The dotted circle in each panel is the position of molecule which moves last in the series of pushing steps. (a) $N_d = 1$. Each push-induced movement is directionally random and independent of its predecessor. (b) $N_d = 3$. The initial and two consecutive movements move in the same direction. Then, the third displacement becomes directionally random, and the two subsequent moves (fourth and fifth moves) take the direction of the third move. This type of pushing continues until there is no molecules left to push out.

To test the RW model, we completed the following MD simulation. DPN is simulated by using nonpolar spherical molecules on a (111) surface of gold-like atoms (Figure 1a).[12] The tip is a cylinder made from 2 264 atoms that are similar in size to silicon and which contains 5 602 molecules, mimicking the fountain-pen tip used in DPN.[13] The molecular mass is similar to that of 1-octadecanethiol (ODT). The intermolecular, molecule-tip atom and molecule-surface atom interactions are all described by Lennard−Jones (LJ) potentials, $U(r) = 4\varepsilon[(\sigma/r)^{12} - (\sigma/r)^6]$.[14] The LJ energy and distance parameters of the tip atom, ε and σ, are those of silicon, 0.4184 kJ/mol and 0.4 nm, respectively.[15] The ε (= 5.24 kJ/mol) of the molecule is taken from that of stearic acid ethyl ester ($C_{20}H_{40}O_2$), which is similar in mass to ODT.[16] The σ (= 0.497 nm) of the molecule is chosen to produce a monolayer geometrically identical to the monolayer of ODT on Au (111).[17] The σ of a surface atom is similar to that of gold (0.2655 nm).[18] The ε for the molecule-surface interaction is taken to be 12.7 kcal/mol, because this gives a monolayer with hexagonal branches.[12] The surface consists of 44 815 atoms and is 1.3 nm below the tip end. The simulation is run for 3 ns by using the velocity Verlet algorithm[14] with a time step of 5 fs. The temperature is fixed to 300 K by using a Berendsen thermostat.[19] More details can be found in ref 12.

We performed a RW simulation emulating the MD simulation as follows. The molecules in MD simulation adsorb to one of three-fold hollow sites of the (111) surface. The trigonal lattice of these hollow sites was first constructed by taking its lattice spacing l (= 0.5385 nm) to be the average distance between the NN molecules of the monolayer in the MD simulation. The trigonal lattice was replicated vertically to give a three-dimensional lattice for the RW simulation. Consequently, each lattice point has two and six NNs in the vertical and lateral directions, respectively. The distances from a lattice point to its eight NNs were all set to l. Each molecule randomly jumps to one of its NN positions. However, the upward jump is excluded because the molecules are attracted down to the surface. The sequence in which each molecule moves is random. When a random jump causes an overlap of the jumper with one of its NN molecules, the neighbor molecule gives up its original position and jumps immediately to one of its own NN positions. If a molecule on the surface is pushed down by a molecule above it, it jumps laterally to one of its six lateral NN positions. If a molecule on the surface is pushed laterally by its NN, it jumps in one of five directions because the direction toward the pusher is excluded. This pushing propagates toward the periphery of the monolayer, and it stops when there is no remaining overlap of molecules. Each column of the droplet was stacked continuously with molecules from the bottom up (no overhangs or vacancies of the column). In a single RW time step dt, all the molecules are randomly moved as described above (therefore, a RW step refers to sweeping moves of all the molecules).

Our RW simulation also requires modeling of the molecular deposition from the tip, which is detailed as follows. The molecules deposited from the tip were defined as those entering the second layer of droplets from the third layer. The deposition rate n is defined as the number of molecules deposited per unit time. n depends on time t and was determined every 1.25 ps of the MD simulation. The monolayer growth distinctly slowed down after 312.5 ps, which naturally divides the growth process into two phases, the launching and the expansion phases.[12] In the initial launching phase (t < 312.5 ps), the molecules were deposited relatively rapidly from the tip because there are few molecules preoccupying the area directly under the tip. In the subsequent expansion phase, t > 312.5 ps, molecular deposition from the tip requires the pushing out of molecules preexisting under the tip and is therefore slower. Figure 3a,c shows representative MD snapshots of the newly deposited molecules in the launching and expansion phases, respectively. Only the surface atoms (drawn small) and molecules that have newly entered the second layer of the droplet are shown (shaded circles). The tip boundary is drawn as a big circle on the periphery. By collecting 2 400 snapshots such as in Figure 3a,c, we constructed histograms for the deposition number n, $h(n)$, as in Figure 3b,d (drawn as open bars). $h(n)$ for the expansion phase, Figure 3d, is shifted toward a lower n and has a narrow distribution compared to that for the launching phase, Figure 3b. We then fitted $h(n)$ to a Poisson distribution of n just as we modeled N_d by using eq 1 (note, incidentally, a random Poisson distribution is used for both N_d and n). A nonlinear fit of $h(n)$ as a Poisson distribution gives average values of n of 6.7 and 1.6 for the launching (Figure 3b) and expansion, (Figure 3d) phases, respectively. The Poisson fit, which is drawn as filled bars in Figure 3b,d, was close to $h(n)$ from MD simulation. In the RW simulation, these Poisson distributions were used to choose n at a given time, and the lateral position of each of the n molecules to deposit was chosen at random within the tip boundary (drawn circular boundaries in Figure 3a,c). Each molecule was placed on top of the molecule preoccupying the lateral position of the previous deposition or directly on the surface if no molecule existed.

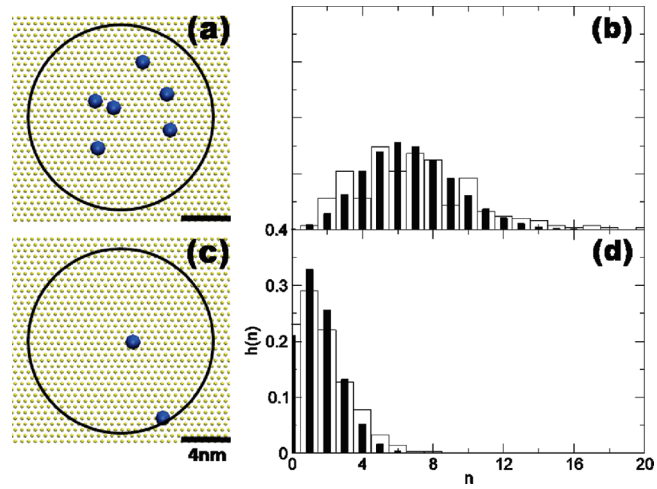

Figure 3. MD snapshots of the molecules newly deposited from the tip and histogram of the number of such molecules. Shown on the left are MD snapshots of molecules deposited in the second layer of a multilayered droplet (top view). The remaining molecules (those not in the second layer or those not newly deposited in the second layer) and tip atoms are not drawn. The tip boundary is shown as a circle. The MD snapshots were taken at times earlier (a) and later (c) than 312.5 ps corresponding to the launching and expansion phases of DPN. On the right, histograms $h(n)$ associated with the number of molecules deposited in the second layer n are plotted as open bars for times earlier (b) and later (d) than 312.5 ps. The filled bars are Poisson distribution fits to $h(n)$. The axis scales in panels c and d are shared by those of a and b, respectively.

As shown above, the molecular deposition is distinctly different for the launching and expansion phases of MD simulation (Figure 3). Therefore, we implemented different RW simulations for the launching and expansion phases. Because the monolayer growth in the launching is isotropic, the serial pushing is taken to be directionally incoherent, $N_d = 0$. We counted the number of RW steps needed to deposit the same number of molecules as that in the MD simulation (1 873 molecules). The RW time step dt was calculated as 1.18 ps. The monolayer in the expansion phase of the MD simulation develops distinct branches. Accordingly, the serial pushing of the RW in this case has a finite directional coherence length N_d. To determine the appropriate N_d, we systematically varied λ in the Poisson distribution for N_d, eq 1, from 5 to 50 with an increment of 5. A λ of 35 was chosen because it showed the best match with the final monolayer pattern in the MD simulation. We then determined the RW time step for the expansion phase by counting the number of dt steps required to deposit the same number of molecules in the MD simulation (3 700 molecules). The resulting dt is 1.13 ps, virtually identical to that in the launching phase.

3. Results and Discussions

Figure 4 shows monolayer growth in the RW simulation in comparison with that of the MD simulation. Snapshots are taken at times of 312.5 ps (Figure 4a,b) and 3 ns (Figure 4c,d). The monolayer at early times was circular and isotropic because of the hopping down and directionally incoherent serial pushing in the growth of a small-sized monolayer. In addition, direct deposition from the laterally circular tip, as shown in Figure 3a,c, increased the circularity of the monolayer at the early times.

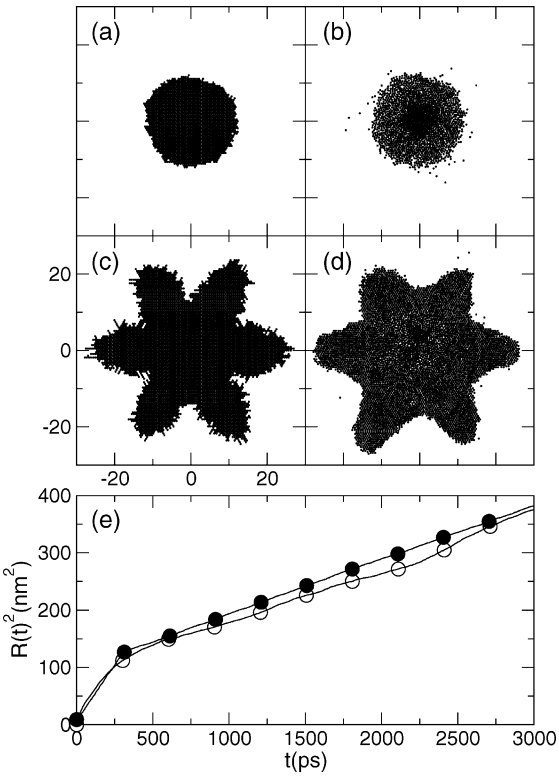

Figure 4. Comparison of monolayer patterns generated by the RW and MD simulations. The monolayer growth in the RW simulation is shown at times of 312.5 ps (a) and 3 ns (c). The corresponding MD simulation snapshots are shown in (b) and (d). The axis scales shown in (c) apply to (a), (b), and (d), and the lengths are in nanometers. In (e), the radius squared of the monolayer $R(t)^2$ is plotted as a function of time t. The open (filled) symbols represent the MD (RW) simulation, respectively. The lines are the actual data, and the symbols are drawn for a visual guide.

As the size of the monolayer increases at later times, the hopping-down event disappears and serial pushing dominates in monolayer growth. The monolayer develops distinct hexagonal branches (Figure 4c) because of the directional coherence of serial pushing (35 molecules, on average, moving in the same direction). Before developing pronounced branches, the monolayer temporarily becomes a hexagon (not shown). The RW simulation closely reproduces the size and shape of the MD monolayer. Quantitatively, Figure 4e shows the effective radius squared of the monolayer $R(t)^2$ (defined as its area divided by π times the monolayer density) for both MD (open circles) and RW (filled circles) simulations. The rate of increase in $R(t)^2$ with respect to time decreases after the initial launching phase (t < 312.5 ps). The RW simulation gave $R(t)^2$ in quantitative accord with the MD result.

We also tried N_d values lower and higher than those in Figure 4. As N_d is changed, the RW model produces a variety of patterns like a circle or a hexagon. Figure 5 shows the monolayers resulting from the Poisson distribution for N_d, eq 1, with λ of 15 (a), 25 (b), 35 (c), and 45 (d). In each case of Figures 5a−d, the molecular deposition from the tip is modeled exactly in the same way as in Figure 3 (by using the Poisson histograms shown in Figure 3b,d). For the lowest directional coherence (an average N_d of 15), the monolayer is circular (Figure 5a). As the average N_d increases from 15 to 25, the circular monolayer changes its shape to a hexagon (Figure 5b). An increase of the average N_d from 25 to 35 develops hexagonal branches as in Figure 5c (which is the replication of Figure 4c). As N_d further increases, the hexagonal branches become

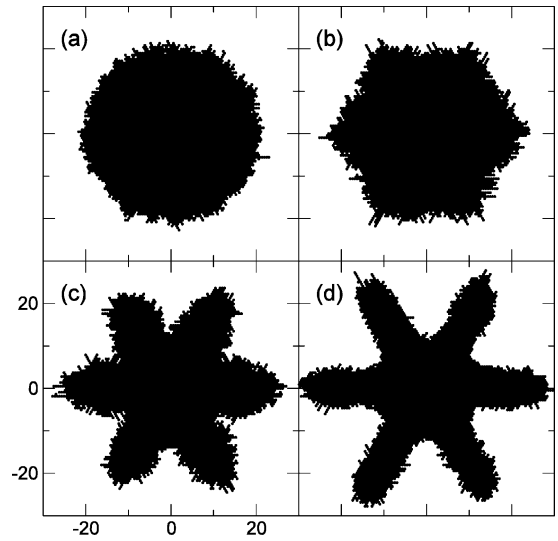

Figure 5. Diverse monolayer patterns produced by the RW model. Like in Figure 4a,c, the directional coherence length is modeled as a Poisson distribution, eq 1. The monolayer patterns are generated by using λ valuess of 15 (a), 25 (b), 35 (c), and 45 (d). Each snapshot is taken just after a total of 5 572 molecules are deposited on the surface. Lengths are in nanometers.

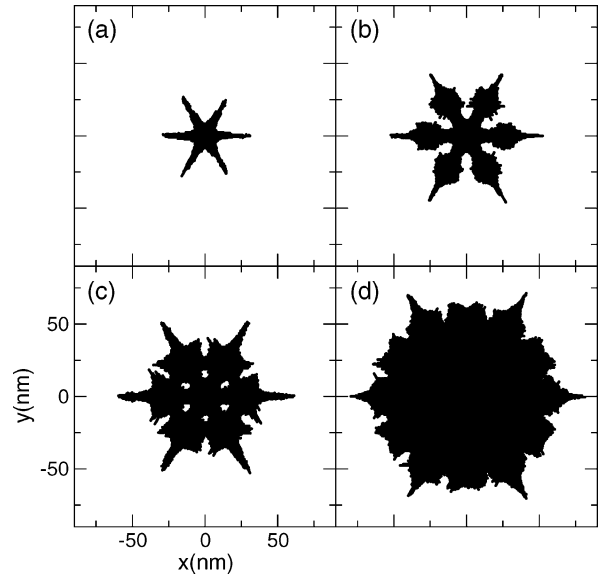

Figure 6. Dendritic growth of monolayer simulated by using the current RW model. The directional coherence is modeled by the Poisson distribution, eq 1, with an average N_d of 50. The tip constantly deposits 10 molecules at a time. The snapshots were taken at 250 (a), 1 000 (b), 1 750 (c), and 5 000 (d) RW time steps.

narrower and more distinct (Figure 5d). These various patterns are also seen in the previous MD simulation by varying the molecule-surface binding energy.[12] Note that simply changing the directional coherence in the RW model produces patterns with various shapes and complexity.

The directional coherence in the RW simulation was further increased to exceed the scope of the MD simulation. Figure 6 shows monolayer growth obtained by using a large N_d value. Here, the tip uniformly deposits 10 molecules at each time, and N_d is 50 on average (Poisson distribution). The snapshots are taken at 250 (a), 1 000 (b), 1 750 (c), and 5 000 (d) RW time steps. As shown in Figure 6a, the hexagonal branches are narrower than those in Figures 4 and 5 because of an enhanced N_d. At 1 000 time steps (Figure 6b), the monolayer evidently develops secondary branches that stem from the original

hexagonal branches. Each of these secondary branches grows in five directions only because the direction toward the center of the monolayer is excluded (pushing always directs away from the center of monolayer). Because of a finite N_d, each of the hexagonal branches changes its growth direction at approximately N_d lattice points away from the center. The secondary branches grow in five equivalent directions because the change in growth direction is random. As a result, those points that are N_d lattice spacings away from the center of the monolayer serve as hubs for secondary branches. These self-developing branches are characteristic of dendritic growth. As the secondary branches grow with time, they are connected to each other, leaving temporary empty spots in the monolayer, as shown in Figure 6c. These vacancy islands in the monolayer are eventually filled in due tobecause of continuous molecular deposition from the center of the monolayer (Figure 6d). The monolayer then loses its pronounced branches and becomes more or less compact with minor branches in its perimeter. With a directional coherence even greater than that in Figure 6, a monolayer can have tertiary, quarternary, and higher-order branches.

The simulation parameters for Figure 6 are set somewhat arbitrarily to demonstrate possible replicating branches of the monolayer. It is not certain to which experimental system the monolayer of Figure 6 corresponds, except that the surface has a hexagonal symmetry and its lattice is commensurate with molecular diameter. If such geometric conditions are met and if the molecular motion shows a large directional coherence as in Figure 6, our simulation predicts that a replicating branch structure should be observed at early times of the monolayer growth.

The present model can serve as a starting point for improved modeling of experimental dendrites in DPN. It can be generalized in two aspects at least. First, note that RWs can be divided into those occurring on and above the surface. For RWs above the surface (in the second or higher layers), it is reasonable to take the lattice spacing for RW to be the molecular diameter because it is the closest approach between two molecules. The lattice spacing for RWs on the surface (first layer), however, is not necessarily identical to the molecular diameter. We assumed that the two lattices (on and above the surface) are commensurate because the Au (111) surface is fairly flat (although it still has hexagonal anisotropy): the molecular diameter of ODT is nearly two times larger than the lattice spacing of Au (111). However, if the surface is rugged as in the case where the molecule is smaller than the lattice spacing of surface, the lattice spacing for RWs on the surface would be incommensurate with (larger than) the molecular diameter. Surface lattices in which the lattice spacing is not the same as the particle diameter would have lost registry in the pushing process and would not preserve the simple structure of the underlying lattice, most likely leading to a loss of coherence and a more irregular monolayer. Second, the Poisson distribution for N_d, eq (1) can be replaced by a broader distribution (e.g., Gaussian) which can increase the irregularity of dendrite.

The hexagonal nature of the branches shown in Figures 4, 5, and 6 arises from the underlying symmetry of the Au (111) surface. The monolayer would have grown four-fold branches instead if a square lattice was used as for the (001) surface of a face-centered cubic crystal. In the case of Au (110), the monolayer would develop branches with a two-fold symmetry because of the rectangular symmetry of the surface. The lattice spacing in one direction would not be commensurate with the molecular diameter, making the branches of monolayer less pronounced. The symmetry of dendrite is therefore determined by that of the surface. This symmetric dendrite structure contrasts with the experimentally observed dendrites that have irregular branches of micrometer dimensions. For a quantitative comparison with experiment, we need to take into account additional details that underlie the experiments. For example, our model should emulate the effects of roughness, defects, and the polycrystallinity (multiple domains) on the surface. Here, we content ourselves with the quantitative agreement of the model with the MD results which are exact within the model potentials.

4. Concluding Remarks

The RW model has been presented on the basis of the simple idea that a monolayer in DPN grows by processes in which the hopping down and serial pushing of molecules are combined. A pronounced branch of a monolayer originates from the directional coherence in serial pushing. The model quantitatively captures the DPN of nonpolar molecules on a gold-like surface, as simulated by the MD method. By simply changing the directional coherence length, the model reproduces a variety of patterns observed in the previous MD simulation, such as a circle and a hexagon with or without branches. As the directional coherence is increased beyond that considered in the MD simulation, the model provides a monolayer with self-replicating multiple-branches characteristic of a dendrite. Unlike conventional dendrites, these replicating branches connect to each other later and disappear if the molecular deposition from the tip continues.

This model represents significant progress over the previous models of DPN, which invariably give compact and isotropic monolayers. It can be implemented easily in the simulation of DPN with a tip moving over a surface. Because of its simplicity, the model should be suitable for simulating DPN for sizes (micrometers) and time scales (>milliseconds) of DPN experiment which are beyond the reach of the molecular simulations. It is encouraging that a mere change in directional coherence produces such a variety of patterns with different complexity ranging from a circle or hexagon to dendrites. We did not however try to reproduce the random and fractal dendrites observed in DPN experiments.[6,7] Our goal here was to show that the model gives self-replicating branches characteristic of dendrites and captures the essential features of MD simulation for thiols on gold. A further improvement of the model and a possible reproduction of experimental dendrites will be the next step. Further improvement is expected by considering the roughness, defects, and directional randomness of the surface, instead of the perfect hexagonal symmetry of the (111) surface assumed here.

The present model should also provide insight to related phenomena, such as the dendritic growth in the microcontact printing[20] and in tip-induced vapor deposition of a film.[20] The hexagonal branches of the monolayer are reminiscent of the growth of a snowflake. In this case, a solid phase grows in the mixture of solid and vapor phases (two-phase growth). We have demonstrated that the monolayer growth in DPN can be formulated as a two-phase growth problem.[10] That is, if the growing monolayer is regarded as a mobile phase, the area outside of the monolayer can be considered as an immobile phase (zero diffusivity). Possibly, we can use various theoretical methods developed for two-phase growth problem, such as the phase-field method.[2,3] This would be another interesting future work.

We note some experimental efforts to understand the molecular transport properties of DPN. A water meniscus forms

between the tip and the surface under humid conditions. It is reported that the water solubility of the molecules and the hydrophilicity of the surface greatly affect the molecular transport.[22] It is also demonstrated that the molecular detachment from the tip is the limiting step in the molecular transport.[23] The molecular detachment from the tip in our simulation is taken to have a constant rate (deposition rate n), and the presence of water meniscus is neglected. We thus excluded the upward jump in RWs. At the molecular time scale (femtoseconds), molecules in principle can move upward because of the molecular detachment and attachment occurring on the tip and the molecular dissolution in the meniscus. The net effects of such processes at the diffusion time scale (picoseconds) would be minor. Nevertheless, it would be interesting to include these experimental findings and investigate how these factors affect the monolayer growth.

When considering the coarse-grained model of thiol, our simulation can be only remotely related to a specific real experiment. Moreover, the exact geometries of tip and surface in experiments are usually unknown. Therefore, we roughly estimate what experiment the present MD simulation corresponds to. The molecular deposition from the tip in simulation has a circular area of 8 nm in radius. This is smaller than but comparable to the radius of a sharpened tip in DPN which can be as small as 12 nm.[24] Our simulation represents a deposition which is spatially more concentrated than that in typical DPN performed by using a blunt tip. A concentrated deposition makes the branches in the monolayer narrower and more pronounced than in typical DPN. Even though we chose the maximal number of molecules that can be simulated when using our computational resource, this number is much smaller than in typical DPN experiment. However, because we are focusing on the short times, the number of molecules deposited per unit time (deposition rate) can be larger than that in DPN experiment.[25]

Acknowledgment. This study was supported by the National Research Foundation Grant funded by the Korean Government (KRF-2008-521-C00123) and by the National Science Foundation (Grant CHE-0843832).

References and Notes

(1) Langer, J. S. *Rev. Mod. Phys.* **1980**, *52*, 1.
(2) Asta, M.; Beckermann, C.; Karma, A.; Kurz, W.; Napolitano, R.; Plapp, M.; Purdy, G.; Rappaz, M.; Trivedi, R. *Acta Materialia* **2009**, *57*, 941.
(3) Boettinger, W. J.; Warren, J. A.; Beckermann, C.; Karma, A. *Annu. Rev. Mater. Res.* **2002**, *32*, 163.
(4) Das, I.; Agrawal, N. R.; Gupta, S. K.; Gupta, S. K.; Rastogi, R. P. *J. Phys. Chem. A* **2009**, *113*, 5296.
(5) Levi, A. C.; Kotrla, M. *J. Phys.: Condens. Matter* **1997**, *9*, 299.
(6) Manandhar, P.; Jang, J.; Schatz, G. C.; Ratner, M. A.; Hong, S. *Phys. Rev. Lett.* **2003**, *90*, 115505.
(7) Rivas-Cardona, J. A.; Banerjee, D. *J. Micro/Nanolith. MEMS MOEMS* **2007**, *6*, 033004.
(8) Salaita, K.; Wang, Y.; Mirkin, C. A. *Nat. Nanotechnol.* **2007**, *2*, 145.
(9) Basnar, B.; Willner, I. *Small* **2009**, *5*, 28.
(10) Jang, J.; Hong, S.; Schatz, G. C.; Ratner, M. A. *J. Chem. Phys.* **2001**, *115*, 2721.
(11) Kim, H.; Jang, J. *J. Phys. Chem. A* **2009**, *113*, 4313.
(12) Heo, D. M.; Yang, M.; Hwang, S.; Jang, J. *J. Phys. Chem. C* **2008**, *112*, 8791.
(13) Kim, K.-H.; Moldovan, N.; Espinosa, H. D. *Small* **2005**, *1*, 632.
(14) Allen, M. P.; Tildesley, D. J. *Computer Simulation of Liquids*; Clarendon Press: Oxford, 1987.
(15) Zhang, L.; Jiang, S. *J. Chem. Phys.* **2002**, *117*, 1804.
(16) Zhou, J.; Lu, X.; Wang, Y.; Shi, J. *Fluid Phase Equlib.* **2000**, *172*, 279.
(17) Alves, C. A.; Smith, E. L.; Porter, M. D. *J. Am. Chem. Soc.* **1992**, *114*, 1222.
(18) Zhang, L.; Balasundaram, R.; Gehrke, S. H.; Jiang, S. *J. Chem. Phys.* **2001**, *114*, 6869.
(19) Berendsen, H. J. C.; Postma, J. P. M.; van Gunsteren, W. F.; DiNola, A.; Haak, J. R. *J. Chem. Phys.* **1984**, *81*, 3684.
(20) Lee, I.; Ahn, J. S.; Hendricks, T. R.; Rubner, M. F.; Hammond, P. T. *Langmuir* **2004**, *20*, 2478.
(21) Zhang, G.; Weeks, B. L. *Scanning* **2008**, *30*, 228.
(22) Hampton, J. R.; Dameron, A. A.; Weiss, P. S. *J. Am. Chem. Soc.* **2006**, *128*, 1648.
(23) Giam, L. R.; Wang, Y.; Mirkin, C. A. *J. Phys. Chem. A* **2009**, *113*, 3779.
(24) Haaheim, J.; Eby, R.; Nelson, M.; Fragala, J.; Rosner, B.; Zhang, H.; Athas, G. *Ultramicroscopy* **2005**, *103*, 117.
(25) Heo, D. M.; Yang, M.; Kim, H.; Saha, L. C.; Jang, J. *J. Phys. Chem. C* **2009**, *113*, 13813.

JP909766P